

Anisotropic Observations in Universes with Nonlinear Inhomogeneity

Neil P Humphreys[†], Roy Maartens^{†*}, and David R Matravers[†]

[†]School of Mathematical Studies, Portsmouth University, Portsmouth PO1 2EG, England

*Member of Center for Nonlinear Studies, Witwatersrand University, 2050 South Africa

Abstract. We calculate the off-center observational relations in a spherically symmetric dust universe that is inhomogeneous at small redshifts. In contrast to the usual model, in which the CMBR dipole is interpreted as a Doppler effect due to peculiar velocity, our model explores an alternative interpretation, in which the CMBR dipole is non-Doppler, and the observer is comoving with the mean matter flow. We do not assume a background frame relative to which peculiar velocities are calculated. Our analysis is fully nonlinear and the density contrast is not assumed to be small. We obtain exact expressions for the Hubble and deceleration parameters, and find that both parameters have quadrupole anisotropies, but no dipoles. A simple numerical procedure for calculating the CMBR dipole anisotropy in our model is presented, and the observed 0.1% dipole is shown to be reproducible with a reasonable choices of parameters.

1. Introduction

Cosmological models with inhomogeneous spherically symmetric regions have been extensively studied (e.g. Wesson 1979; Raine and Thomas 1981; Lynden-Bell *et al.* 1988; Bertschinger and Juszkiewicz 1988; Bertschinger and Dekel 1989; Panek 1992; Mészáros 1994; Moffat and Tatarski 1995; Tomita 1995). With some exceptions (e.g. Tomita and Watanabe 1989; Paczynski and Piran 1990; Arnau *et al.* 1994), the inhomogeneity in the matter is generally treated as a perturbation of a homogeneous background, which restricts the analysis to small density contrast and small peculiar gravitational potential in a linearised theory. The CMBR dipole is then interpreted as a Doppler effect arising from our peculiar motion relative to the background.

Linearised inhomogeneous models with a position-dependent Hubble parameter H_0 can be used to explain why measurements of H_0 (see Riess *et al.* (1995) and Van den Bergh (1995) for recent results) tend to give relatively high values from methods dependent on local observations, and lower values from methods based on more distant observations. (The Hubble parameter relevant to large-scale cosmology should be low to avoid contradiction between the universal age calculated from H_0 and Ω_0 , and the limits due to the age of constituents of the universe).

In this paper the inhomogeneity is treated self-consistently, without linearised perturbations, thus allowing for nonlinear peculiar gravitational potential and density contrast (while also incorporating the case of small density perturbations). We therefore consider cosmological models which may be homogeneous on large scales, but which can incorporate arbitrary isotropic inhomogeneity on smaller scales (say about 100 Mpc). In order to exploit the possibilities of such models, while simultaneously exploring alternatives to the standard models, we take the dipole anisotropy of the CMBR, and any anisotropies in the Hubble and deceleration parameters, to arise not from the observer's peculiar motion (relative to some background), but from the observer's off-center location, i.e. from the inhomogeneous gravitational field. Galaxies follow unperturbed motion in this field, so from their viewpoint there is no peculiar velocity. For comoving observers away from the center of symmetry, the CMBR dipole anisotropy will be interpreted as a cosmological effect, rather than the effect of local peculiar motion. A similar model of the CMBR dipole was given by Paczynski and Piran (1990), and

non-Doppler dipoles arising from large-scale perturbations were considered by Bildhauer and Futamase (1991), and Langlois and Piran (1995). The CMBR itself cannot distinguish between these two interpretations. Indeed, the observer's peculiar velocity is not directly observed, but postulated as a reasonable source of the CMBR dipole. Our model thus investigates an alternative explanation.

As pointed out by Paczynski and Piran (1990), observations have not decisively established the reality of large-scale departures from a mean Hubble flow, so that alternative models of the CMBR dipole can help to develop new ways of testing the standard model. It turns out that both H_0 and q_0 in our model (i.e. a freely falling off-center observer) have *no* dipole anisotropy, whereas the standard model (i.e. peculiar motion towards a Great-Attractor-like structure) does predict dipoles in H_0 and q_0 (cf. Nakao *et al.* 1995). Thus, in principle, measurements of H_0 via the distance-redshift observations could distinguish between these alternatives.

Exact formulas for the Hubble and deceleration parameters are given in §4. These arise from the local solution of the null-geodesic equation near the off-center observer, as discussed in §2. In §5 we show how to calculate the CMBR dipole, and in the appendix the observed value is obtained using a reasonable choice of cosmological parameters.

2. Off-Center Geometry

The Lemaître-Tolman-Bondi (LTB) metric (Bondi 1947) gives the geometry corresponding to a spherically symmetric space-time with a pressure-free dust matter distribution, prior to the formation of shell-crossing singularities:

$$ds^2 = -dt^2 + \frac{R'(r,t)^2}{1+f(r)} dr^2 + R(r,t)^2 (d\theta^2 + \sin^2 \theta d\phi^2) \quad (1)$$

where $x^0 \equiv t$ is cosmic proper time and $x^i \equiv \{r, \theta, \phi\}$ are comoving. The arbitrary function f determines the curvature of the spatial hypersurfaces. The units are chosen such that $c = G = 1$, and the cosmological constant $\Lambda = 0$. Einstein's field equations reduce to

$$\dot{R}^2 = \frac{2M(r)}{R} + f \quad (2)$$

$$\rho = \frac{M'}{4\pi R' R^2} \quad (3)$$

where ρ is the proper density, and $M(r)$ is the gravitational mass inside the sphere of radius r . A prime denotes $\partial/\partial r$, and a dot $\partial/\partial t$. The four-velocity of the dust is $u^\mu = \delta_0^\mu$.

Let P_0 label the spacetime event of an off-center observer at time $t = t_0$, i.e. the event $\{t = t_0, r = r_0, \theta = \pi/2, \phi = 0\}$.

With k^μ the tangent to the geodesics $x^\mu(v)$, the geodesic equations $k^\mu{}_{;\nu} k^\nu = 0$ take the form

$$\frac{d^2 t}{dv^2} + \frac{\dot{R}' R'}{1+f} \left(\frac{dr}{dv}\right)^2 + \dot{R} R L^2 = 0 \quad (4)$$

$$\frac{d^2 r}{dv^2} + 2 \frac{\dot{R}'}{R'} \frac{dt}{dv} \frac{dr}{dv} + \left(\frac{R''}{R'} - \frac{f'}{2(1+f)}\right) \left(\frac{dr}{dv}\right)^2 - (1+f) \frac{R}{R'} L^2 = 0 \quad (5)$$

$$\frac{d^2 \theta}{dv^2} + 2 \frac{\dot{R}}{R} \frac{d\theta}{dv} \frac{dt}{dv} + 2 \frac{R'}{R} \frac{dr}{dv} \frac{d\theta}{dv} - \sin \theta \cos \theta \left(\frac{d\phi}{dv}\right)^2 = 0 \quad (6)$$

$$\frac{d^2 \phi}{dv^2} + 2 \frac{\dot{R}}{R} \frac{d\phi}{dv} \frac{dt}{dv} + 2 \frac{R'}{R} \frac{dr}{dv} \frac{d\phi}{dv} + 2 \cot \theta \frac{d\theta}{dv} \frac{d\phi}{dv} = 0 \quad (7)$$

where $L^2 \equiv (d\theta/dv)^2 + \sin^2 \theta (d\phi/dv)^2$. The first integral

$$-\left(\frac{dt}{dv}\right)^2 + \frac{R'^2}{1+f} \left(\frac{dr}{dv}\right)^2 + R^2 L^2 = 0 \quad (8)$$

specifies that the geodesics are null. If the choice $v = 0$ at P_0 is made, then the past null-geodesics through P_0 are locally expressible as

$$x^\alpha(v) = \sum_{n=0}^3 (x^\alpha)_n v^n + O(v^4) \quad (9)$$

and the functions R and f may similarly be assumed Taylor-expandable. Throughout the paper a subscript ‘0’ denotes evaluation at P_0 . The geodesic equations (4-7) may be solved locally by equating coefficients of powers of v . The solution is of the form $\{r_2, r_3, \dots, t_2, t_3, \dots, \theta_2, \theta_3, \dots, \phi_2, \phi_3, \dots\}$ with each coefficient a function of the observational angles ϑ and φ at P_0 .

Since affine parameters remain affine under linear transformations, v may be fixed by choosing

$$t_1 = -1 \tag{10}$$

This choice forces v to increase down geodesics of incoming light, and is equivalent to setting $u_\mu k^\mu = 1$ at P_0 (Ellis *et al.* 1985). Evaluation of equation (8) to lowest order in v results in

$$r_1 = (-1)^\epsilon \left[\frac{\sqrt{1+f}}{R'} \sqrt{1 - R^2(\theta_1^2 + \phi_1^2)} \right]_0 \tag{11}$$

The factor $\epsilon = 0$ (or 1) is determined by the motion of rays at P_0 toward (or away) from the center of symmetry.

Equations (8) and (11) are equivalent, since geodesics that are initially null must remain null. The four components of k^μ at P_0 may be interpreted as follows: t_1 fixes the gauge of the affine parameter by equation (10), r_1 specifies the geodesics are null by equation (11), and θ_1 and ϕ_1 determine the 2-sphere of observer angles $\{\vartheta, \varphi\}$ at P_0 .

Calculation of ϑ and φ in terms of θ_1 , ϕ_1 , and ϵ , is as follows. Let I^μ , J^μ , and K^μ be unit vectors in the surface $\{t = t_0\}$, with I^μ pointing radially outward from the center of symmetry, K^μ pointing in the direction associated with $-\partial/\partial\theta$, and J^μ pointing in the direction of an observed light ray:

$$I^\mu = \left[\frac{\sqrt{1+f}}{R'} \delta_r^\mu \right]_0 \tag{12}$$

$$J^\mu = \left(0, \frac{\sqrt{(1+f)[1 - R^2(\theta_1^2 + \phi_1^2)]}}{R'}, \theta_1, \phi_1 \right)_0 \tag{13}$$

$$K^\mu = - \left[\frac{1}{R} \delta_\theta^\mu \right]_0 \tag{14}$$

Let ϑ and φ be defined (relative to θ , ϕ , and ϵ) via

$$\epsilon = 0 = \phi_1 \Leftrightarrow \varphi = 0, \quad \theta_1 = 0 \Leftrightarrow \vartheta = \frac{\pi}{2} \tag{15}$$

Then φ is given by $\cos \varphi = I^\mu J_\mu$ with $\theta_1 = 0$, which yields

$$\varphi = \epsilon\pi + (-1)^\epsilon \arcsin(R\phi_1)_0 \tag{16}$$

Also $\cos \vartheta = J^\mu K_\mu$ implies

$$\vartheta = \arccos(-R\theta_1)_0 \tag{17}$$

Equations (16) and (17) invert to

$$\phi_1 = \left[\frac{\sin \varphi}{R} \right]_0, \quad \theta_1 = - \left[\frac{\cos \vartheta}{R} \right]_0 \tag{18}$$

Now, by spherical symmetry, just one angle is required to describe the off-center observations: the angle ψ between I^μ and the direction of observation at P_0 . Observations with common ψ must be indistinguishable. Attention may therefore be restricted to the plane $\{\theta(v) = \pi/2 = \vartheta\}$, for which $\psi = \varphi$.

3. Matching Constraints

We require that the inhomogeneous models become homogeneous on a sufficiently large distance scale. For simplicity it is supposed that the transition occurs on a well-defined comoving spherical boundary without any

surface density layer (Israel 1966). The coordinates x^μ may be extended beyond the boundary (at $r = \chi$, say) and into the external FLRW region. For $r < \chi$ the inhomogeneous LTB solution is

$$f = 0 : \quad R = (9M/2)^{\frac{1}{3}} (t - \beta)^{\frac{2}{3}} \quad (19)$$

$$f > 0 : \quad R = M (\cosh \eta - 1) / f, \quad \sinh \eta - \eta = f^{\frac{3}{2}} (t - \beta) / M \quad (20)$$

$$0 > f > -1 : \quad R = M (\cos \eta - 1) / f, \quad \eta - \sin \eta = |f|^{\frac{3}{2}} (t - \beta) / M \quad (21)$$

in the parabolic, hyperbolic, and elliptic cases respectively. The function $\beta(r)$ gives the big-bang hypersurface. For $r > \chi$ the homogeneous LTB (FLRW) solution is

$$f = 0 : \quad R = (9Mt^2/2)^{\frac{1}{3}} \quad (22)$$

$$f = \alpha (2M)^{\frac{2}{3}} > 0 : \quad R = (\cosh \eta - 1) (M/4\alpha^3)^{\frac{1}{3}}, \quad \sinh \eta - \eta = 2\alpha^{\frac{3}{2}} t \quad (23)$$

$$0 > f = -\alpha (2M)^{\frac{2}{3}} > -1 : \quad R = (1 - \cos \eta) (M/4\alpha^3)^{\frac{1}{3}}, \quad \eta - \sin \eta = 2\alpha^{\frac{3}{2}} t \quad (24)$$

where α is a constant, and the large-scale FLRW Hubble and density parameters are given by

$$f = 0 : \quad \mathcal{H} = 2/3t, \quad \Omega = 1 \quad (25)$$

$$f > 0 : \quad \mathcal{H} = 2\alpha^{\frac{3}{2}} \sinh \eta / (\cosh \eta - 1)^2, \quad \Omega = 2 (\cosh \eta - 1) / \sinh^2 \eta \quad (26)$$

$$0 > f > -1 : \quad \mathcal{H} = 2\alpha^{\frac{3}{2}} \sin \eta / (1 - \cos \eta)^2, \quad \Omega = 2 (1 - \cos \eta) / \sin^2 \eta \quad (27)$$

The boundary hypersurface has intrinsic metric $K_{\mu\nu} = g_{\mu\nu} - n_\mu n_\nu$ and extrinsic curvature $n_{\mu;\nu} K_\alpha^\mu K_\beta^\nu$, where n_μ is the unit normal. The Darmois junction conditions (for the case with no surface layer at $r = \chi$) are (Israel 1966) that the intrinsic metric and the extrinsic curvature, evaluated on the two sides of $r = \chi$, are equal. Restricting attention to solutions which have the same characteristic curvatures (parabolic, hyperbolic, or elliptic) on both sides of $r = \chi$, the conditions are

$$\text{all } f : \quad \lim_{\delta \rightarrow 0} [M(\chi + \delta) - M(\chi - \delta)] = 0 \quad (28)$$

$$f = 0 : \quad \beta(\chi) = 0 \quad (29)$$

$$f > 0 : \quad \beta(\chi) = 0, \quad f(\chi) = \alpha [2M(\chi)]^{\frac{2}{3}} \quad (30)$$

$$0 > f > -1 : \quad \beta(\chi) = 0, \quad f(\chi) = -\alpha [2M(\chi)]^{\frac{2}{3}} \quad (31)$$

Papapetrou (1978) successfully matched an interior collapsing ($f < 0$) LTB solution to the Einstein-de Sitter model (for which $f = 0$). It may also be possible to obtain an internal LTB solution consisting of several zones with different solution branches ($f < 0, f = 0, f > 0$), obeying the Darmois conditions on their concentric spherical interfaces. These are however highly non-trivial models, in which the avoidance of shell-crossing caustics is a difficult problem. (When dust shells cross the zero-pressure condition of LTB is violated). An analysis of some of the issues relating to the matching of LTB solutions will be the subject of subsequent research.

4. Off-Center Observations: Galaxies

In this paper, idealised cosmological observations are assumed. In particular, it is supposed that area distances (or equivalently luminosity distances) and number counts are known as functions of the redshift. Hence any statistical, averaging, smoothing, and distance-dependent selection effects are neglected. As is well known (Maartens *et al.* 1996) LTB models are completely specified by complete measurements of the area distance and number count as functions of the redshift. In what follows, these two functions are expanded about P_0 , up to the first two non-vanishing derivatives in the redshift.

The redshift z as measured at P_0 is given by $1 + z = u^\mu k_\mu$ (Ellis *et al.* 1985), and by equation (10):

$$z = -\frac{dt(v)}{dv} - 1 \quad (32)$$

The observer area distance D at P_0 may be obtained by considering an observational coordinate system (Ellis *et al.* 1985) at P_0 . The observational coordinates are $\tilde{x}^\mu \equiv \{w, v, \vartheta, \varphi\}$, where $\{w = \text{constant}\}$ are the past light cones from the observer's world-line at P_0 . The metric tensor in observational coordinates is then

$$\tilde{g}_{\mu\nu} = g_{\alpha\gamma} \frac{\partial x^\alpha}{\partial \tilde{x}^\mu} \frac{\partial x^\gamma}{\partial \tilde{x}^\nu} \quad (33)$$

Thus the angular part of the transformed metric $\tilde{g}_{\vartheta\vartheta}, \tilde{g}_{\varphi\varphi}, \tilde{g}_{\vartheta\varphi}$ on the past-light cone of P_0 can be calculated locally from the null-geodesic solution and equations (18). Then D follows from the formula (Ellis *et al.* 1985)

$$D^4 \sin^2 \vartheta = \tilde{g}_{\vartheta\vartheta} \tilde{g}_{\varphi\varphi} - (\tilde{g}_{\vartheta\varphi})^2 \quad (34)$$

Equation (34) and the local null-geodesic solution lead to

$$\left(\frac{dD}{dz}\right)_0 = \frac{1}{\mathcal{C}_1 + \mathcal{C}_2 \cos^2 \psi} \quad (35)$$

$$\left(\frac{d^2D}{dz^2}\right)_0 = \frac{\mathcal{C}_3 + \mathcal{C}_4 |\cos \psi| + \mathcal{C}_5 \cos^2 \psi + \mathcal{C}_6 |\cos \psi|^3}{(\mathcal{C}_1 + \mathcal{C}_2 \cos^2 \psi)^3} \quad (36)$$

where the constants \mathcal{C}_I are given in the appendix.

The Hubble parameter H of a spherically symmetric inhomogeneous universe is often given two definitions (e.g. Moffat and Tatarski 1995):

$$H_r = \dot{R}/R, \quad H_\phi = \dot{R}'/R' \quad (37)$$

which are to be interpreted as radial and azimuthal expansion rates (generally the expansion is anisotropic since the shear is non-vanishing). The two definitions agree at the center of symmetry, as follows from equation (2) and the behaviours of f , M , and R near the center (Bondi 1947):

$$R(r, t) = R'(0, t)r + O(r^2), \quad f(r) = \frac{1}{2}f''(0)r^2 + O(r^3), \quad M(r) = \frac{1}{6}M'''(0)r^3 + O(r^4) \quad (38)$$

Using equations (37), we obtain

$$H_\phi(0, t) = R'(0, t)^{-1} \sqrt{M'''(0)/6R'(0, t) + \frac{1}{2}f''(0)} = H_r(0, t) \quad (39)$$

Moffat and Tatarski (1995) have posed the question of which one is the analogue of the FLRW H_0 , when off-center. We resolve this issue by the use of a covariant definition:

$$H_0 = \frac{1}{\delta l} \frac{d(\delta l)}{dt} \quad (40)$$

where δl is the proper distance from P_0 to neighbouring worldlines. This leads to (Ehlers 1993)

$$H_0 = \left[\frac{1}{3}\Theta + \sigma_{\mu\nu} J^\mu J^\nu \right]_0 \quad (41)$$

where

$$\Theta = u^\mu{}_{;\mu} = \frac{\dot{R}'}{R'} + 2\frac{\dot{R}}{R} \quad (42)$$

is the rate of volume expansion, and

$$\sigma_{\mu\nu} = u_{(\mu;\nu)} - \frac{1}{3}\Theta(g_{\mu\nu} + u_\mu u_\nu) + u_{(\mu} u_{\nu);\lambda} u^\lambda \quad (43)$$

is the rate of shearing. For the LTB metric (eq. [1]), this gives

$$\sigma_1^1 = \frac{2}{3} \left(\frac{\dot{R}'}{R'} - \frac{\dot{R}}{R} \right), \quad \sigma_2^2 = \sigma_3^3 = -\frac{1}{2}\sigma_1^1 \quad (44)$$

with all other σ_ν^μ vanishing. Equations (41-44), (13), and (18) result in

$$H_0 = \mathcal{C}_1 + \mathcal{C}_2 \cos^2 \psi \quad (45)$$

Definition (40) is equivalent to the (covariant) definition of H_0 as the initial slope of the redshift–area distance curve:

$$H_0 = \left(\frac{dz}{dD} \right)_0 \quad (46)$$

as may be seen from equation (35). The deceleration parameter q_0 may be covariantly defined as (*cf.* Partovi and Mashhoon 1984; Kantowski *et al.* 1995; Dabrowski 1995)

$$q_0 = -H_0 \left(\frac{d^2 D}{dz^2} \right)_0 - 3 \quad (47)$$

and using equation (36) this results in

$$q_0 = -\frac{\mathcal{C}_3 + \mathcal{C}_4 |\cos \psi| + \mathcal{C}_5 \cos^2 \psi + \mathcal{C}_6 |\cos \psi|^3}{(\mathcal{C}_1 + \mathcal{C}_2 \cos^2 \psi)^2} - 3 \quad (48)$$

The above formulae for H_0 and q_0 are exact covariant generalisations of the FLRW definitions. Note that neither of the expressions possess a dipole. In principle, they provide an observational test of these models against the peculiar velocity–type models which do predict dipoles. Typical values of the \mathcal{C}_I for Great–Attractor data are given in the appendix.

The galactic number count N (per steradian at P_0) is in general dependent on the direction of observation. Furthermore, the total integrated number count over all angles and out to some distance, will depend on the distance definition used (redshift, area–distance, \dots). One may obtain N (considered as a function of ϑ and φ) from¹ equation (19) of Ellis *et al.* (1985):

$$dN = snD^2(1+z)dv \quad (49)$$

where n is the proper number density of galaxies and s is the selection factor (mean fraction of galaxies that are detectable). In general s varies down the null–geodesics; here it is assumed constant since such observational problems are not the focus of this paper. The function n is determined by $n = \rho/m$, where m is the mean galactic mass (assumed constant) and ρ is given by equation (3). Equation (49) and the local null–geodesic solution lead to

$$\left(\frac{d^3 N}{dz^3} \right)_0 = \left(\frac{s}{4\pi m} \right) \frac{\mathcal{C}_7}{(\mathcal{C}_1 + \mathcal{C}_2 \cos^2 \psi)^3} \quad (50)$$

$$\left(\frac{d^4 N}{dz^4} \right)_0 = \left(\frac{s}{4\pi m} \right) \frac{\mathcal{C}_8 + \mathcal{C}_9 |\cos \psi| + \mathcal{C}_{10} \cos^2 \psi + \mathcal{C}_{11} |\cos \psi|^3 + \mathcal{C}_{12} \cos^4 \psi}{(\mathcal{C}_1 + \mathcal{C}_2 \cos^2 \psi)^5} \quad (51)$$

where the constants \mathcal{C}_I are in the appendix. The first two derivatives of N with respect to z vanish, by equation (49). Note that, like H_0 and q_0 , these N - z relations do not contain any dipoles.

The luminosity distance D_L is (Ellis *et al.* 1985)

$$D_L = D(1+z)^2 \quad (52)$$

All derivatives of D , N , and D_L with respect to z at P_0 may be calculated in principle. However, high–order derivatives are of no practical interest as they are well beyond the bounds of current observational sensitivity. Given the assumption $z \ll 1$ on the boundary $\{r = \chi\}$, the model is well–characterised by ideal observations expanded as far as their first two non–vanishing powers in the redshift.

¹Equation (19) of Ellis *et al.* (1985) has an error: the RHS should be multiplied by dv/dy .

5. Off–Center Observations: CMBR

In this section we present a numerical procedure for calculating the CMBR anisotropy, and in the appendix the dipole is evaluated in a special case.

To obtain the dipole in the anisotropy, it is supposed that there exists a well–defined last scattering surface from which the CMBR is emitted isotropically, so that we exclude the effect on the CMBR of processes at decoupling, in order to focus on the purely gravitational effect of the nonlinear matter inhomogeneity (*cf.* Raine and Thomas 1981; Tomita and Watanabe 1989; Arnau *et al.* 1994). We also ignore the anisotropies arising from inhomogeneous regions other than our own (in the ‘Swiss cheese’ model, see Arnau *et al.* (1994) for detailed calculations). The calculated dipole anisotropy is thus due to the off–center location of the observer in the inhomogeneous region (figure 1). We do not calculate the quadrupole (or higher multipole moments), as the inhomogeneous–matter contribution to the CMBR quadrupole is expected to be swamped by effects at decoupling (see Nakao *et al.* (1995) for estimates in the case of an observer with peculiar motion).

The dipole anisotropy may be calculated for an off–center observer by noting that the first two terms of the multipole temperature expansion are T and $\Delta T \cos \psi$. Calculation of the difference in redshift of CMBR rays along $\{\psi = 0\}$ and $\{\psi = \pi\}$ then suffices to obtain $\Delta T/T$. These trajectories are the radial null–geodesics:

$$\frac{dt(r)}{dr} = (-1)^{\epsilon+1} \frac{R'[r, t(r)]}{\sqrt{1+f(r)}} \quad (53)$$

With (53), (32), and $L \equiv 0$, equation (4) expresses the redshift as

$$\left[\frac{1}{1+z(r)} \right] \frac{dz(r)}{dr} = (-1)^\epsilon \frac{\dot{R}[r, t(r)]}{\sqrt{1+f(r)}} \quad (54)$$

The coupled first order o.d.e.s, (53) and (54), are readily solved numerically, with initial data $\{z(r_0) = 0, t(r_0) = t_0\}$. In the hyperbolic and elliptic cases (eq. [20–21]) we do not have $R[r, t(r)]$ explicitly. For numerical purposes, we write instead $R[r, \eta(r)]$ and solve equations (53–54) coupled with a third o.d.e.:

$$\frac{d\eta(r)}{dr} = \dot{\eta}[r, \eta(r)] \frac{dt(r)}{dr} + \eta'[r, t(r), \eta(r)] \quad (55)$$

The cosmological scenario under consideration in this paper is illustrated in figure 1. Let the proper times at events A , C , and X be denoted t_A , t_C , and t_X . The redshift between P_0 and event X (event C) is z_X (z_C), and z_{AX} is that between A and X . The FLRW redshift z_{BC} between B and C is given by

$$1 + z_{BC} = \left\{ \begin{array}{ll} (t_C/t_B)^{\frac{2}{3}} & (f = 0) \\ (\cosh \eta_C - 1) / (\cosh \eta_B - 1) & (f > 0) \\ (\cos \eta_C - 1) / (\cos \eta_B - 1) & (0 > f > -1) \end{array} \right\} \equiv \left(\mathcal{H}^{\frac{2}{3}} \Omega^{\frac{1}{3}} \right)_B \quad (56)$$

and by $t_B = t_A$. The parameter η is defined in equations (22–24).

Now the redshift in the $\psi = 0$ direction, minus the redshift in the opposite direction is

$$\Delta z = (1 + z_C) (1 + z_{BC}) - (1 + z_X) (1 + z_{AX}) \quad (57)$$

and the exact expression for the temperature dipole anisotropy is

$$\frac{\Delta T}{T} = \frac{1}{2} \left\{ (1 + z_C)^{-1} (1 + z_{BC})^{-1} - (1 + z_X)^{-1} (1 + z_{AX})^{-1} \right\} \quad (58)$$

which is approximately $-\Delta z/2$ for small redshifts.

For numerical calculations, the gauge freedom in the radial coordinate should be removed. Assuming a finite and non–zero proper density, equation (2) implies $M(r) = O(r^3)$ for small r . Therefore the coordinate freedom in r may be removed by choosing a mass–coordinate:

$$2M(r) = r^3 \quad (59)$$

such that the remaining (non–trivial) arbitrariness in the dust solution (given by two arbitrary functions; Bondi 1947), corresponds to physically distinct models.

Equations (53–59) give a simple procedure for CMBR dipole calculation. A numerical example is given in the appendix, reproducing the observed 0.1% dipole for a reasonable choice of parameters.

6. Discussion

In §4 we obtained that the angular dependences of H_0 , q_0 , d^3N/dz^3 , and d^4N/dz^4 are functions of $|\cos\psi|$, and hence have no dipole components in their multipole expansions. Since idealised observations taken further than their second non-vanishing redshift derivatives (d^3D/dz^3 , etc.) are well beyond the sensitivity of current observational data, it can be concluded that all current idealised galactic observations should reveal no dipole dependences, if our model is a valid description of the real universe. If dipoles were observed, our model would fall away, and the peculiar-velocity models would be strengthened.

In the appendix, the main results of this paper are illustrated by application to the Great-Attractor data. The Hubble parameter result

$$H_0 \approx (45 + 12 \cos^2 \psi) \text{ kms}^{-1}\text{Mpc}^{-1} \quad (60)$$

shows a quadrupole term with an amplitude of $\approx 12\%$ of the magnitude of the monopole. We emphasise that the existence of a quadrupole component in H_0 (and in q_0) has nothing in common with ‘correcting’ H_0 for any ‘peculiar velocity’ (such as that defined by the CMBR dipole). Furthermore, the quadrupole cannot be removed by any such Lorentz transformation at P_0 , since the corresponding correction to H_0 is dipolar and not quadrupolar (Nakao *et al.* 1995). The GA data, whilst having considerable standard deviation, do represent a reasonable local geometry, and suggest that the angular variations of H_0 and q_0 are not negligible in many physically acceptable cosmologies.

The set of physically independent arbitrary parameters at P_0 is $\{\dot{R}, R, R', R'', f, f', f''\}$. The mass out to P_0 is given by \dot{R} , but higher time derivatives are not independent, due to the field equation (2). This set of seven parameters can be related to a set of seven independent observed parameters by an algebraic inversion. For brevity, the result of the calculation is not given in this paper. Note however that one possible choice of seven independent observed parameters is $\{\mathcal{C}_1, \mathcal{C}_2, \mathcal{C}_3, \mathcal{C}_4, \mathcal{C}_7, \mathcal{C}_9, \mathcal{C}_{11}\}$.

In LTB models, the quadrupole term in H_0 vanishes along off-center comoving world-lines when $\mathcal{C}_2 = 0$. This reduces to the pair of conditions

$$(\beta')_0 = 0, \quad \left[f' - f(4/M)^{\frac{1}{3}} \right]_0 = 0 \quad (61)$$

which imply (in one sense) that the universe is locally FLRW: the first implies that in the comoving frame, the big-bang was locally simultaneous at $r = r_0$; the second implies that either $f = 0$ (corresponding to the Einstein-de Sitter model), or that at $r = r_0$ the radial gradients of the gravitational mass M and total energy W ($W \equiv \sqrt{1+f}$, Bondi 1947) are related by

$$\frac{3W}{W^2 - 1} dW = \frac{dM}{M} \quad (62)$$

which is satisfied for all r in FLRW models. Hence if the quadrupole vanishes everywhere, the universe must be the FLRW model.

Wesson (1979) considered an exact self-similar dust solution (a special case of LTB), and obtained expressions for the observables. This paper may be considered a generalisation of Wesson (1979), since for the special case he considered,

$$R(r, t) = r \left[\frac{3}{2}(\alpha_s + t/r) \right]^{\frac{2}{3}}, \quad f(r) = 0 \quad (63)$$

his results follow from those here. Note however that here the full angular dependences of the observations are given (Wesson considered only the azimuthal and radial directions), and that here the luminosity distance-redshift relation and number count-redshift relation are considered, as opposed to Wesson’s (equivalent) magnitude-redshift and number density-redshift relations.

While the off-center position of the observer removes many of the simplifications imposed by isotropy, spherical symmetry remains a special case of inhomogeneity. However, assuming that local inhomogeneities are spherically symmetric is a first step towards the study of realistic inhomogeneities and their impact on observations.

Appendix

a. Specific Models using Great-Attractor Data

The Great-Attractor (GA) is generally assumed to cause a perturbation of the homogeneous background which lies in the linear regime (*cf.* Panek 1992). Data for the attractor is typically in the form of a peculiar velocity field V . In particular, Lynden-Bell et al. (1988) give

$$V = V_0 S_0 (S^{-1})_{t=t_0} \quad (64)$$

where S is radial proper distance from the GA, $S_0 \approx 87$ Mpc, $V_0 \approx -570$ kms $^{-1}$, and we take $\mathcal{H}_0 = 50$ kms $^{-1}$ Mpc $^{-1}$. Quantitative density estimates are far more speculative.

In the small density contrast and small peculiar gravitational potential limit of our model, we may identify

$$V = \left(\dot{R} - \mathcal{H}R \right)_{t=t_0} \quad (65)$$

and $R \approx S$. Note that there is no unique generalisation of equation (65) to the fully nonlinear case. In our model, V is not a peculiar velocity, but is used to fix numerical values in the model.

Hence we require an inhomogeneous LTB model which is specified by equations (64) and (65), and an assumed density distribution. Note however, that equation (64) will be simulated only approximately, since the matching conditions require $V = 0$ at $r = \chi$. Also equation (64) is singular at the center, whereas we shall require $V = 0$ there, on physical grounds. One possible inhomogeneous model that fits these observational constraints is the elliptic solution given by

$$0 > f(r) = -\alpha r^2 \{1 - \lambda_1 [\exp(-\lambda_2 r^2/\chi^2) - \exp(-\lambda_2)]\} \quad (66)$$

$$\beta(r) = \lambda_3 [\exp(-\lambda_4 r^2/\chi^2) - \exp(-\lambda_4)] \quad (67)$$

which matches to the closed FLRW solution (24) at $r = \chi$, with r the mass-coordinate [eq. (59)]. The constants λ_I are given by

$$\lambda_1 = 80, \quad \lambda_2 = 0.43, \quad \lambda_3 \approx 1.96 \times 10^{17} \text{s}, \quad \lambda_4 = 0.25 \quad (68)$$

and we choose $\alpha \approx 1.32 \times 10^{-13} \text{s}^{-\frac{2}{3}}$, so that $\Omega_0 = 1.1$. The proper radius out to $r = \chi$ is chosen to be ≈ 96.9 Mpc. The ratio of the inhomogeneous proper density to the homogeneous background density $\rho/\bar{\rho}$, is plotted in figure 2, and figure 3 gives the CMBR dipole. From the plots, the observed 0.1% dipole occurs at a radius of ≈ 80 Mpc, where the proper density is $\approx 4 \times 10^{-30} \text{gcm}^{-3}$.

The (mathematically simpler) parabolic case is inappropriate for description of the GA (in our model), as it predicts a cold spot in the direction of the GA. The problem is that the rate of expansion near the GA is greater than in the FLRW region. Interpreted via the peculiar velocity function V , this means V is positive (in the direction *away* from the GA). We can see this quantitatively as follows. The density ratio is

$$\frac{\rho}{\bar{\rho}} = \frac{t^2}{(t - \beta - \frac{2}{3}r\beta')(t - \beta)} \quad (69)$$

We must have $\beta'(r) \leq 0$ for $r < \chi$, to avoid singular densities for $t - \beta > 0$. From (29), $\beta(\chi) = 0$, hence the function β must be everywhere positive, and the peculiar velocity

$$V = \mathcal{H}_0 r \left(\frac{9}{4} \right)^{\frac{1}{3}} (t_0 - \beta)^{-\frac{1}{3}} \beta \quad (70)$$

must also be positive.

It is however possible to use the $f = 0$ assumption to estimate the observational parameters (\mathcal{C}_I), as they are affected only by the local metric, and there is no evidence to rule out $f \approx 0$ locally to P_0 . Hence we take $S = R + \varepsilon$, where ε corrects for the deviation of S from R near the GA, and is approximately constant on the time slice $\{t = t_0\}$ near P_0 . The total mass out to distance S_0 from the GA is $\approx 5 \times 10^{47}$ kg (Panek 1992).

This fixes the mass-coordinate at P_0 , and the observed parameters \mathcal{C}_I may be obtained from appendix (b) and by equating spatial derivatives of equations (64) and (65) at P_0 . The results are

$$\left. \begin{array}{l} \mathcal{C}_1 = +45 \\ \mathcal{C}_2 = +12 \end{array} \right\} \text{kms}^{-1}\text{Mpc}^{-1}, \quad \left. \begin{array}{l} \mathcal{C}_3 = -0.02 \\ \mathcal{C}_4 = -0.4 \\ \mathcal{C}_5 = -0.01 \\ \mathcal{C}_6 = +0.6 \end{array} \right\} \text{kms}^{-1}\text{Mpc}^{-2}, \quad (71)$$

$$\mathcal{C}_7 = +4000 \text{ kgkm}^{-2}\text{Mpc}^{-1}, \quad \left. \begin{array}{l} \mathcal{C}_8 = -200 \\ \mathcal{C}_9 = -9000 \\ \mathcal{C}_{10} = -200 \\ \mathcal{C}_{11} = +10^5 \\ \mathcal{C}_{12} = +5 \end{array} \right\} \text{kgMpc}^{-3}\text{km}^{-1}\text{s}^{-1} \quad (72)$$

b. Coefficients

The coefficients in equations (36–51) are (implicit evaluation at P_0)

$$\begin{aligned} \mathcal{C}_1 &= \frac{\dot{R}}{R} \\ \mathcal{C}_2 &= \frac{\dot{R}'}{R'} - \frac{\dot{R}}{R} \\ \mathcal{C}_3 &= \frac{\ddot{R}}{R} - \frac{3\dot{R}^2}{R^2} \\ \mathcal{C}_4 &= 3\sqrt{1+f} \left(\frac{\dot{R}}{R^2} - \frac{\dot{R}'}{R'R} \right) \\ \mathcal{C}_5 &= \frac{3\dot{R}^2}{R^2} - \frac{3\dot{R}'^2}{R'^2} - \frac{\ddot{R}}{R} + \frac{\ddot{R}'}{R'} \\ \mathcal{C}_6 &= \sqrt{1+f} \left(\frac{3\dot{R}'}{RR'} + \frac{\dot{R}'R''}{R'^3} - \frac{3\dot{R}}{R^2} - \frac{\dot{R}''}{R'^2} \right) \\ \mathcal{C}_7 &= \frac{\dot{R}^2}{R^2} - \frac{f}{R^2} + \frac{2\dot{R}\dot{R}'}{RR'} - \frac{f'}{RR'} \\ \mathcal{C}_8 &= -\frac{9\dot{R}^4}{R^4} + \frac{9\dot{R}^2 f}{R^4} - \frac{24\dot{R}'\dot{R}^3}{R'R^3} + \frac{12\dot{R}^2 f'}{R'R^3} + \frac{6\dot{R}'\ddot{R}\dot{R}}{R^2 R'} - \frac{6\dot{R}^2 \ddot{R}'}{R^2 R'} + \frac{6\dot{R}^2 \dot{R}'^2}{R^2 R'^2} - \frac{3f'\dot{R}'\dot{R}}{R'^2 R^2} - \frac{6f\ddot{R}}{R^3} - \frac{6f'\ddot{R}'}{R'R^2} \\ \mathcal{C}_9 &= 3\sqrt{1+f} \left(-\frac{4f\dot{R}}{R^4} + \frac{6f\dot{R}'}{R^3 R'} + \frac{4\dot{R}^3}{R^4} - \frac{f''\dot{R}}{R'^2 R^2} - \frac{10\dot{R}\dot{R}'^2}{R^2 R'^2} - \frac{2\dot{R}^2 \dot{R}'R''}{R^2 R'^3} + \right. \\ &\quad \left. + \frac{R''f'\dot{R}}{R^2 R'^3} + \frac{6f'\dot{R}'}{R'^2 R^2} + \frac{6\dot{R}^2 \dot{R}'}{R^3 R'} - \frac{6f'\dot{R}}{R'R^3} + \frac{2\dot{R}^2 \dot{R}''}{R^2 R'^2} \right) \\ \mathcal{C}_{10} &= -\frac{6f'\ddot{R}'}{R'^2 R} + \frac{15f'\dot{R}'^2}{R'^3 R} - \frac{12\dot{R}f\dot{R}'}{R^3 R'} + \frac{18f\dot{R}'^2}{R^2 R'^2} - \frac{6f\ddot{R}'}{R^2 R'} - \frac{6\dot{R}'^2 \ddot{R}}{RR'^2} - \frac{30\dot{R}\dot{R}'^3}{RR'^3} + \frac{6\dot{R}\ddot{R}'\dot{R}'}{RR'^2} - \frac{6\dot{R}^2 f}{R^4} + \\ &\quad - \frac{6\dot{R}^2 \dot{R}'^2}{R^2 R'^2} - \frac{6f'\dot{R}'\dot{R}}{R^2 R'^2} + \frac{30\dot{R}'\dot{R}^3}{R'R^3} - \frac{9\dot{R}^2 f'}{R^3 R'} - \frac{12\dot{R}'\ddot{R}\dot{R}}{R^2 R'} + \frac{12\dot{R}^2 \ddot{R}'}{R^2 R'} + \frac{6f\ddot{R}}{R^3} + \frac{6f'\ddot{R}'}{R^2 R'} + \frac{6\dot{R}^4}{R^4} \\ \mathcal{C}_{11} &= -3\sqrt{1+f} \left(\frac{4f\dot{R}'}{R^3 R'} - \frac{4f\dot{R}}{R^4} + \frac{2f\dot{R}'R''}{R'^3 R^2} - \frac{2f\dot{R}''}{R'^2 R^2} - \frac{2\dot{R}\dot{R}'^2 R''}{RR'^4} - \frac{f''\dot{R}}{R^2 R'^2} + \frac{6f'\dot{R}'}{R^2 R'^2} - \frac{2\dot{R}^3}{RR'^3} - \frac{2f'\dot{R}''}{RR'^3} + \right. \\ &\quad \left. + \frac{f''\dot{R}'}{RR'^3} + \frac{R''f'\dot{R}}{R^2 R'^3} + \frac{2\dot{R}\dot{R}'\dot{R}''}{RR'^3} + \frac{4\dot{R}^2 \dot{R}''}{R^2 R'^2} - \frac{6f'\dot{R}}{R'R^3} + \frac{4\dot{R}^3}{R^4} + \frac{f'\dot{R}'R''}{RR'^4} - \frac{10\dot{R}\dot{R}'^2}{R^2 R'^2} - \frac{4\dot{R}^2 \dot{R}'R''}{R'^3 R^2} + \frac{8\dot{R}^2 \dot{R}'}{R^3 R'} \right) \\ \mathcal{C}_{12} &= \frac{3\dot{R}^4}{R^4} - \frac{3\dot{R}^2 f}{R^4} + \frac{6\dot{R}\dot{R}'^3}{RR'^3} - \frac{3f'\dot{R}'^2}{R^3 R'} - \frac{9\dot{R}^2 \dot{R}'^2}{R^2 R'^2} - \frac{3\dot{R}^2 f'}{R^3 R'} - \frac{3f\dot{R}'^2}{R^2 R'^2} + \frac{6\dot{R}f\dot{R}'}{R^3 R'} + \frac{6\dot{R}'\dot{R}f'}{R^2 R'^2} \end{aligned}$$

References

- Arnau, J. V., Fullana M. J., and Sáez, D., 1994, *M. N. R. A. S.*, **268**, L17.
- Bertschinger, E., and Dekel, A., 1989, *Ap. J.*, **336**, L5.
- Bertschinger, E., and Juszkiewicz, R., 1988, *Ap. J.*, **334**, L59.
- Bildhauer, S., and Futamase, T., 1991, *M. N. R. A. S.*, **249**, 126.
- Bondi, H., 1947, *M.N.R.A.S.*, **107**, 410.
- Dabrowski, M. P., 1995, *Ap. J.*, **447**, 43.
- Ehlers, J., 1993, *Gen. Rel. Grav.*, **25**, 1225 (translation of original 1961 article).
- Ellis, G. F. R., Nel, S. D., Maartens, R., Stoeger, W. R., and Whitman, A. P., 1985, *Phys. Rep.*, **124**, 315.
- Israel, W., 1966, *Nuovo Cimento*, **44B**, 1.
- Kantowski, R., Vaughan, T., and Branch, D., 1995, *Ap. J.*, **447**, 35.
- Langlois, D., and Piran, T., 1995, preprint astro-ph.
- Lynden-Bell, D., Faber, S. M., Burstein, D., Davies, R. L., Dressler, A., Terlevich, R. J., and Wegner, G., 1988, *Ap. J.*, **326**, 19.
- Maartens, R., Humphreys, N. P., Matravers, D. R., and Stoeger, W. R., 1996, *Class. Quant. Grav.*, in press.
- Mészáros, A., 1994, *Ap. J.*, **423**, 19.
- Moffat, J. W., and Tatarski, D. C., 1995, *Ap. J.*, **453**, 17.
- Nakao, K., Gouda, N., Chiba, T., Ikeuchi, S., Nakamura, T., and Shibata, M., 1995, *Ap. J.*, **453**, 541.
- Paczynski, B., and Piran, T., 1990, *Ap. J.*, **364**, 341.
- Panek, M., 1992, *Ap. J.*, **388**, 225.
- Papapetrou, A., 1978, Ann. L'Institut Henri Poincaré, **A**, XXIX, 2, 207.
- Partovi, M. H., and Mashhoon, B., 1984, *Ap. J.*, **276**, 4.
- Raine, D. J., Thomas, E. G., 1981, *M. N. R. A. S.*, **195**, 649.
- Riess, A. G., Press, W. H., and Kirshner, R. P., 1995, *Ap. J.*, **438**, L17.
- Tomita, K., 1995, *Ap. J.*, **451**, 1.
- Tomita, K., and Watanabe, K., 1989, *Prog. Theor. Phys.*, **82**, 563.
- Van den Bergh, S., 1995, *Ap. J.*, **453**, L55.
- Wesson, P. S., 1979, *Ap. J.*, **228**, 647.

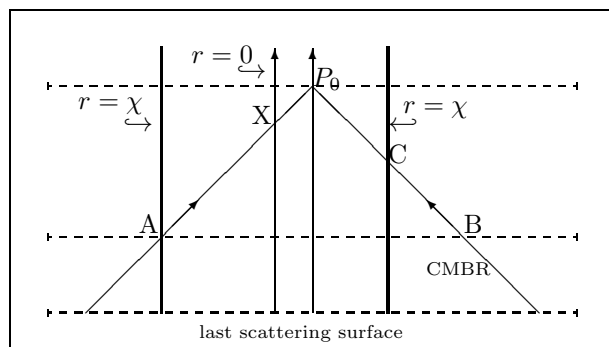
Figure Captions

Figure 1. Schematic for the dipole anisotropy. The frequencies of the two CMBR rays are equal at A and B , but are then redshifted differently on arrival at P_0 . The dotted lines denote constant- t hypersurfaces.

Figure 2. Plot of the density ratio $\rho/\bar{\rho}$ against radial proper distance S for the elliptic GA model (eq. [66–67]) at time $t = t_0$.

Figure 3. Plot of the CMBR temperature dipole $\Delta T/T$ against radial proper distance S for the elliptic GA model (eq.[66–67]) at time $t = t_0$.

FIGURE 1



This figure "fig1-1.png" is available in "png" format from:

<http://arxiv.org/ps/astro-ph/9602033v1>

This figure "fig1-2.png" is available in "png" format from:

<http://arxiv.org/ps/astro-ph/9602033v1>